I&EC research
Industrial & Engineering Chemistry Research

pubs.acs.org/IECR
Article

Promotion of Cobalt Oxide Catalysts by Acid-Etching and Ruthenium Incorporation for Chlorinated VOC Oxidation

Amaya Gil-Barbarin, José Ignacio Gutiérrez-Ortiz, Rubén López-Fonseca,* and Beatriz de Rivas

Cite This: *Ind. Eng. Chem. Res.* 2024, 63, 3003−3017

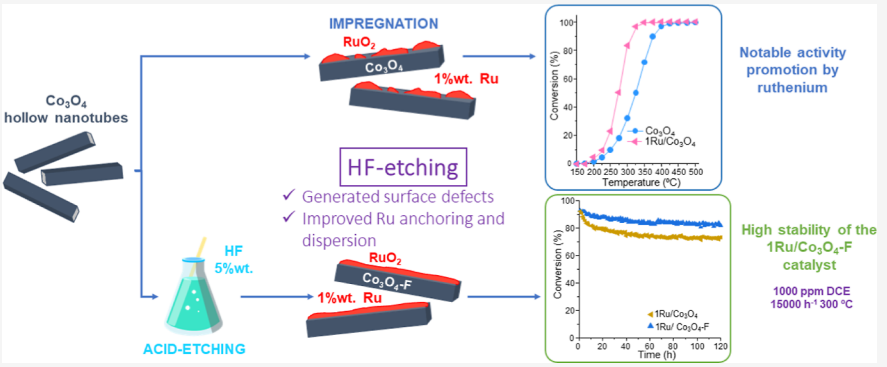

ABSTRACT: In this work, Ru-promoted cobalt oxide catalysts with a nanotube morphology were prepared by a synthesis route based on the Kirkendall effect followed by an acid treatment and subsequent optimized Ru impregnation. The resulting samples were thoroughly characterized by means of N_2 physisorption, X-ray energy-dispersive spectroscopy, X-ray diffraction, scanning electron microscopy techniques, X-ray photoelectron spectroscopy, and temperature-programmed techniques (O_2-temperature-programmed desorption, H_2-temperature-programmed reduction, and temperature-programmed oxidation) and evaluated in the gas-phase oxidation of 1,2-dichloroethane. It has been demonstrated that Ru addition improves the oxygen mobility as well as the amount of Co^{2+} and O_{ads} species at the surface by the formation of the Ru−O−Co bond, which in turn governs the performance of the catalysts in the oxidation reaction. Moreover, the acid-etching favors the dispersion of the Ru species on the surface of the catalysts and strengthens the interaction among the noble metal and the cobalt oxide, thereby improving the thermal stability of the Ru-promoted oxides. Thus, the resulting catalysts are not only active, as the chlorinated pollutant is efficiently converted into deep oxidation products at relatively low temperatures, but also quite stable when operating for 120 h.

1. INTRODUCTION

Emissions of chlorinated volatile organic compounds (Cl-VOCs) have increased in recent years due to the development of modern industry. Along with the environmental impacts (increase in photochemical smog, generation of ground-level ozone, and depletion of stratospheric ozone), the negative effects on human health caused by these emissions have led to the search for technologies for the control and removal of these compounds.[1,2] Among the available processes (adsorption, membrane separation, thermal incineration, and biodegradation), catalytic oxidation is presented as an optimal strategy, owing to its high efficiency in the elimination of trace amounts of Cl-VOCs at relatively low temperatures.[3]

In this sense, the choice of a suitable catalyst (in terms of activity, selectivity toward deep oxidation products, and stability) is essential. Bulk transition-metal oxides, especially Mn, Cu, Fe, or Co oxides, have been extensively applied in Cl-VOC oxidation as a result of their notable catalytic activity and low cost compared with noble metal catalysts.[4−6] Particularly, cobalt-based catalysts have exhibited excellent results in several catalytic processes related to environmental protection.[6−9] The high catalytic activity of this oxide is attributed to its high bulk oxygen mobility, surface area, abundant defects, and the easy formation of highly active oxygen vacancies.[10,11] However, these oxides present some drawbacks such as its slow oxidation−reduction and a high chlorination activity.[12] To overcome these problems, incorporation of controlled amounts of promoters may be applied.[10,12] Noble metals are considered as a good alternative since the amount to be used as a promoter is eventually small, which would not make the catalyst much more expensive. Nonetheless, some of the most commonly used noble metals (Pt and Pd) are very sensitive to

Received: November 16, 2023
Revised: January 26, 2024
Accepted: February 1, 2024
Published: February 13, 2024

https://doi.org/10.1021/acs.iecr.3c04045
Ind. Eng. Chem. Res. 2024, 63, 3003−3017

Cl poisoning which greatly decreases their stability in the oxidation of chlorinated compounds. On the contrary, ruthenium has been widely applied in the gas-phase oxidation of HCl to Cl_2 owing to the remarkable dechlorination efficiency of Ru species.[13] Thus, the Cl species generated from the cleavage of the C−Cl bonds during the oxidation of the chlorinated hydrocarbon are favorably removed from the catalyst surface as Cl_2 owing to the activity of Ru in the Deacon reaction ($2HCl + 1/2O_2 \rightarrow Cl_2 + H_2O$). Moreover, Ru is relatively inexpensive (2−3 times cheaper than Pt and 5−6 times less expensive than Pd), and it has been shown to be quite active in the catalytic oxidation of light hydrocarbons such as propane.[14] However, RuO_x is known to be thermally unstable, leading to volatilization of Ru species in catalytic oxidation processes at high temperatures and resulting in catalysts with poor stability when operating for a long time.[15]

In this sense, the beneficial role of the promoter in terms of enhanced stability relies on its dispersion and interaction with the active phase. Several strategies can be followed to modulate promoter-active phase interactions: tune the characteristics of the bulk oxide acting as a support for the promoter (by altering its morphology and/or chemical composition), change the features of noble metal (by controlling its particle size), and modify the overall structure of the promoted oxide catalyst (by thermal treatment with controlled atmospheres).[16] It has been demonstrated that structural defects on the support surface boost metal−support interaction. Zhang et al. showed that oxygen vacancies in TiO_2 led to strong metal−support interaction between Cu and the support and enhanced the hydrogenation reaction of CO_2 to methanol.[17] Similarly, Wan et al. found that surface oxygen vacancies were appropriate sites to anchor single atomic metal sites.[18] As well as oxygen vacancies, steps on the support have higher adsorption energy and enhanced the interaction between metal particles and support compared with terraces or smooth surfaces, as revealed by Gong et al.[19] In conclusion, the introduction of defects in the support could improve metal−support interactions by enhancing the covalent bonds between the active metal and the support.[15] There are numerous methods available for this purpose, among which acid-etching is a widely employed technique to modulate surface composition and create structural defects on metal oxides.[20,21]

Thus, in this work, Co_3O_4 and Ru-promoted Co_3O_4 catalysts were synthesized and examined for the gas phase removal of 1000 ppm of 1,2-dichloroethane (DCE) as a model-chlorinated VOC. The cobalt oxide support was etched with an aqueous HF solution (5 wt %) to generate surface defects for ruthenium oxide stable anchoring. Subsequently, Ru was deposited on the etched support (0.5, 0.75, and 1 wt %) by an impregnation method to enhance the activity of cobalt oxide in the catalytic removal of chlorinated VOCs. The as-synthesized oxides were extensively characterized by several techniques including N_2 physisorption, energy-dispersive X-ray spectroscopy (EDX), X-ray diffraction (XRD), Raman spectroscopy, scanning electron microscopy (SEM), high-angle annular dark field scanning transmission electronic microscopy (STEM-HAADF), temperature-programmed reduction with hydrogen (H_2-TPR), temperature-programmed desorption of oxygen (O2-TPD), temperature-programmed oxidation (TPO) with oxygen, and X-ray photoelectron spectroscopy (XPS).

2. EXPERIMENTAL METHODS

2.1. Synthesis of the *x*Ru/Co_3O_4−F Catalysts. The preparation of the catalysts involved three consecutive steps, namely, the synthesis of the parent bulk cobalt oxide, its modification by acid-etching and finally the incorporation of the noble metal (Ru).

2.1.1. Preparation of the Co_3O_4 Samples. For the preparation of the Co_3O_4 nanotubes by the Kirkendall effect, a 0.03 M ethanolic solution of cobalt acetate tetrahydrate (Alfa Aesar) was prepared, to which a 0.17 M ethanolic solution of urea (Fluka) was added under stirring. This mixture was kept under stirring for 4 h at 65 °C using a jacketed reactor with reflux to maintain the temperature. Next, the suspension was cooled and then filtered (0.22 μm) to obtain the cobalt hydroxyacetate precursor. The solid was washed with ethanol three times and then dried in an oven at 80 °C for at least 12 h. Finally, the precursor was calcined using a rotary furnace with a flow of 500 $cm^3\ min^{-1}$ of a 5%O_2/He stream. The temperature was first increased to 350 °C using a heating ramp of 1 °C min^{-1} and then kept for 3 h. During the heating process, the oxidation of the C, H, and Co atoms of the Co acetate hydroxide occurred first on the surface of the precursor. In this way, a film of Co_3O_4 was formed on the surface and the newly exposed C, H, and Co atoms emigrated to the surface to react with the oxygen. This process was repeated with the continuous outflow to the surface of the cobalt acetate hydroxide, resulting in the formation of cavities and the subsequent generation of the hollow Co_3O_4 nanotubes. At this temperature (350 °C), the transformation into Co_3O_4 was expected to be fully achieved. However, the oxide was subjected to a new calcination process at 500 °C to produce a thermally stabilized catalyst under the selected reaction conditions for DCE oxidation. This second calcination step was carried out using a heating rate of 1 °C min^{-1} followed by an isothermal event for 3 h (500 °C).[22]

2.1.2. Acid Modification of the Co_3O_4. Once the Co_3O_4 nanotubes were obtained, the next step was the acid treatment of these nanotubes. For this purpose, 1 g of the oxide was taken and placed in a beaker to which 2 mL of 1.25 M HF solution was added. The beaker was then placed in an ultrasonic bath for 30 min at room temperature. The content of the beaker was subsequently filtered to recover the modified Co_3O_4 and washed with distilled water several times to remove any remaining acid solution. Finally, it was dried in an oven at 110 °C overnight. Finally, it was calcined in a muffle furnace under static air conditions at 500 °C using a heating ramp of 1 °C min^{-1}. This temperature was maintained for 3 h. The resulting sample was named as Co_3O_4−F.

2.1.3. Incorporation of Ruthenium. The last step to produce the fully formulated catalysts was the incorporation of ruthenium by means of an optimized impregnation method. Hence, an adjusted amount of $RuCl_3$ (Alfa Aesar) was weighed to achieve the desired Ru content (the Ru/Co_3O_4 mass ratios were 0.5:100, 0.75:100, and 1:100) and then dissolved in distilled water to obtain a 0.2 M solution. Then, a certain volume (10, 15, or 20 mL) of 15% H_2O_2 (Sigma-Aldrich) was added dropwise under stirring, using a peristaltic pump with a flow rate of 5 $cm^3\ min^{-1}$. This solution was then transferred to a water bath where the temperature was raised up to 95 °C. The system was kept under stirring at this temperature for 2 h (with a reflux system to avoid evaporation of water) to obtain the RuO_2 suspension. After this time interval, the suspension

https://doi.org/10.1021/acs.iecr.3c04045
Ind. Eng. Chem. Res. 2024, 63, 3003−3017

was cooled, and the Co_3O_4 powder was added to the mixture. Subsequently, the mixture was heated to 50 °C and kept under stirring at this temperature for 24 h.[23] Afterward, the samples were dried in a rotary evaporator with a rotation speed of 20 rpm at 40−50 °C. Finally, they were calcined in a muffle furnace under static air conditions at 500 °C using a heating ramp of 1 °C min^{-1} and maintained under isothermal conditions for 3 h. The as-synthesized catalysts were denoted as *x*Ru/Co_3O_4−F, where x is the Ru loading of the sample. For comparative purposes, a reference catalyst was also prepared (1Ru/Co_3O_4). In this case, the cobalt oxide nanotubes were not previously treated with HF.

2.2. Characterization Techniques. Textural properties of the obtained samples were examined by N_2 physisorption at the temperature of liquid nitrogen (−196 °C). The experiments were carried out in a Micromeritics TRISTAR II 3020 instrument, and the specific surface area and mean pore size were calculated using the Brunauer−Emmett−Teller (BET) and Barrett−Joyner−Halenda methods, respectively. Prior to the analysis, the samples were degassed at 200 °C for 10 h with N_2 flow. The structural properties of the synthesized catalysts were examined by XRD in powder and Raman spectroscopy. XRD diffraction patterns were taken on an automatic diffractometer model X'Pert PRO from PANalytical using Cu Kα radiation (λ = 1.5406 Å) and a Ni filter at 40 kV and 40 mA. The measurement conditions were optimized to an angular range between 5 and 80° at 2θ with a step size of 0.026° and counting time of 498.3 s per step. International Centre for Diffraction Data (ICDD) database cards were employed for phase identification. Raman spectra were collected on a Renishaw InVia Raman spectrometer using a 514 nm laser source (ion-argon laser, Modu-Laser) and a Leica 50 × Plan lens, scanning from 150 to 1500 cm^{-1}. For each spectrum, 20 s were employed, and 10 scans were accumulated with 10% of the maximum power in the spectral window (2 mW).

The external morphology of the synthesized oxides was studied by means of SEM. For each measurement, a small amount of powdered sample was taken and deposited on a carbon strip in a sample holder. SEM images were obtained on a Hitachi S-4800 scanning electron microscope with cold cathode field emission gun at a working voltage of 10 kV and 5 A. The microscope was equipped with a high-resolution CCD camera. Scanning transmission electron microscopy-high angle annular dark field (STEM-HAADF) images with elemental maps were obtained on a ThermoFisher Scientific/FEI Titan electron microscope operating at 300 kV and equipped with a CESCOR Cs CEOS corrector and Oxford Instruments Ultim Max EDX detector. All these components were operated with a Fischione HAADF detector in the STEM mode. Before the measurement, the samples were sonicated in ethanol and dropped on an amorphous carbon film supported on a copper grid. The collected maps were presented in the form of a matrix of colored pixels with the intensity corresponding to the amount of the element.

Redox properties of the catalysts were evaluated by means of H_2-TPR. The analyses were performed on a Micromeritics Autochem 2920 instrument equipped with a thermal conductivity detector (TCD) detector. Previous to the analysis, the sample was pretreated in a 5%O_2/He stream at 300 °C for 1 h and then cooled to room temperature. Subsequently, a stream of 50 cm^3 min^{-1} of 5%H_2/Ar was flown through the sample from room temperature to 500 °C (10 °C min^{-1}) and maintained for 0.5 h. A cold trap was employed to prevent water generated by the reduction step from interfering with the TCD detector. In order to provide more information about the nature of the mobile oxygen species, O_2-temperature-programmed desorption experiments were also carried out on the same apparatus. Before the analysis, the sample (100 mg) was pretreated in 5%O_2/He stream at 500 °C for 15 min and then cooled to 50 °C. Next, after being purged with helium for 0.5 h, the catalyst was heated to 900 °C for 0.5 h with a heating ramp of 10 °C min^{-1} while following the signal of the desorbed oxygen (m/z = 32) with a Hidden HPR 20 EGA mass spectrometer.

The surface chemical composition was evaluated by X-ray photoelectronic spectroscopy (XPS). The measurements were conducted on a Kratos AXIS Supra spectrometer using 120 W Al Kα monochromatic radiation source with a pass energy of 160 eV for the general survey and 20 eV for the specific spectra. The spectra were adjusted using CasaXPS 2.3.16 software, which models Gauss-Lorentzian contributions, after a background subtraction (Shirley). The concentrations were calculated by correcting the values with relative atomic sensitivity factors (Scofield).

X-ray energy-dispersive spectroscopy (EDX) and TPO were employed to evaluate the eventual chlorine accumulation and coke generation over the used catalysts. EDX results were obtained on a JEOL JSM-6400 scanning electron microscope coupled to an INCA EDX X-sight Si Series (Li) pentaFET Oxford detector with window and INCA 350 data acquisition and power processing allowing accurate, online, and mapped analysis. EDX spectra were measured at 20 kV, 1 nA, and at a working distance of 10 mm. The samples were deposited on an amorphous carbon film supported on a copper grid and placed inside the microscope under high vacuum. TPO analyses were conducted in the TGA 550 thermobalance. The thermobalance was coupled to a Pffeifer Vacuum DUO 2.5 mass spectrometer. Previously to the oxidation process, all the samples (100 mg) were pretreated in a 5%O_2/He flow at 110 °C for 1 h. Subsequently, the temperature was increased to 800 °C with a heating rate of 10 °C min^{-1}, and this temperature was held for 0.5 h.

2.3. Catalytic Behavior Evaluation. The catalytic activity of the catalysts was determined in a bench-scale fixed bed reactor (MICROACTIVITY-Reference MAPXL1M6 model, supplied by PID Eng&Tech S.L.) fully monitored by a computer. For each experiment, 0.85 g of the catalyst (0.08−0.16 mm) was diluted with quartz (0.5−0.8 mm) up to a total volume of 2 cm^3. The catalytic bed was introduced into a quartz reactor of 300 mm length and 10 mm internal diameter, in which a K-type thermocouple was inserted for temperature control. The reactor was fed with 1000 ppm of DCE diluted in 500 cm^3 min^{-1} of dry air. The corresponding weight (WHSV) and gas (GHSV) hourly space velocities were 35,000 mL g^{-1} h^{-1} and 15,000 h^{-1}, respectively. The feeding of the gaseous reagents was controlled by mass flow controllers (EL-FLOW from Bronkhorst High-Tech B.V.) while a syringe pump (kdScientific 200) was used to feed the DCE and water (runs under humid conditions). The position of the liquid injection was electrically heated to ensure the complete evaporation of the reactants. To avoid possible fluctuations in the inlet stream, before reaching the reactor, the feed was homogenized in a 2 L mixer. Catalytic activity was measured from 150 to 500 °C in steps of 25 °C, and conversion data were taken at steady state. For the analysis of molecular chlorine and hydrogen chloride,

https://doi.org/10.1021/acs.iecr.3c04045
Ind. Eng. Chem. Res. 2024, 63, 3003−3017

Table 1. Textural, Structural, and Redox Properties of the Modified Co_3O_4 Catalysts[a]

catalyst	Ru content, wt % (EDX)	S_{BET}, $m^2\ g^{-1}$	V_{pore}, $cm^3\ g^{-1}$	d_{pore}, Å	$D_{Co_3O_4}$, nm (XRD)	$D_{Co_3O_4}$, nm (STEM-HAADF)	low-T reduction peak, °C	high-T reduction peak, °C	O_2 desorbed at low T, μmol g^{-1}
Co_3O_4		19	0.05	200	22	n.a.	260	330	41
$1Ru/Co_3O_4$	1.0	16	0.04	160	25	n.a.	160	245	63
Co_3O_4–F		9	0.02	190	35	n.a.	260	335	40
$0.5Ru/Co_3O_4$–F	0.5	10	0.03	200	37	31	140	225/265	52
$0.75Ru/Co_3O_4$–F	0.6	10	0.03	200	36	32	140	220/260	49
$1Ru/Co_3O_4$–F	0.9	10	0.02	180	36	34	145	230/270	60

[a]n.a.: not analyzed.

both volumetric and potentiometry methods were employed, respectively.[22]

3. RESULTS AND DISCUSSION

3.1. Physical-Chemical Characterization of Co_3O_4 and $1Ru/Co_3O_4$ Catalysts. Textural properties of the synthesized catalysts were evaluated by N_2 physisorption. The adsorption/desorption isotherms as well as the pore size distributions are displayed in Figure S1, Supporting Information. The bare Co_3O_4 showed a type IV isotherm with type H1 hysteresis loop at a relative pressure of P/P_0 = 0.85, typical of mesoporous solids with cylindrical channels.[24] After the incorporation of ruthenium (presumably in the form of RuO_x), no relevant differences in the type of isotherm or hysteresis cycle were found, suggesting that the mesoporous structure was mostly retained upon Ru impregnation. A bimodal pore size distribution was found, where small pores around 25 Å were due to the inner of the nanoparticles; meanwhile, the larger pores around 300 Å were originated by the agglomeration of the nanoparticles.[25] Results of BET surface area, pore volume, and mean pore diameter are shown in Table 1. The Ru-modified sample exhibited a slightly lower surface area (16 $m^2\ g^{-1}$) and pore volume (0.04 $cm^3\ g^{-1}$), probably due to the partial blockage of the cobalt oxide (19 $m^2\ g^{-1}$, 0.05 $cm^3\ g^{-1}$) pores. As estimated by EDX, the Ru content was 1 wt %.

The XRD patterns of the samples are presented in Figure 1. Both bare Co_3O_4 and $1Ru/Co_3O_4$ catalysts exhibited the same diffraction peaks corresponding to the cubic Co_3O_4 oxide at 2θ = 19.2, 31.4, 37.0, 38.7, 45.0, 55.8, 59.5, and 65.4°, which were identified with the (111), (220), (311), (222), (400), (422), (511), and (440) planes, respectively (ICDD 00-042-1467). No diffraction peaks related to the CoO phase or other impurities were visible. For the $1Ru/Co_3O_4$ sample, no diffraction peaks corresponding to ruthenium or ruthenium oxides were detected, possibly due to the low concentration of the metal and its high dispersion on the surface.[11] By applying the Scherrer equation to the diffraction peak associated with the (311) crystal plane, the average crystallite size was estimated (Table 1). The crystallite size was 22 nm on pure Co_3O_4 and slightly larger on $1Ru/Co_3O_4$ catalyst (25 nm).

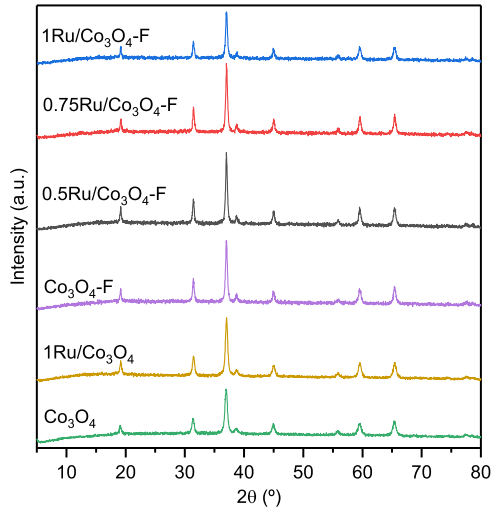

Figure 1. XRD patterns of the modified Co_3O_4 samples.

The external morphology of the catalysts was examined by SEM (Figure 2). The Co_3O_4 sample (Figure 2a) exhibited a reasonably uniform prism morphology. From the images of the broken areas, the desired hollow interior of the tubes could be distinguished. These nanotubes were approximately 2–3 μm in length and 0.5 μm in width. Besides, it is remarkable that the walls of the nanotubes were made of the assembly of nanoparticles of a few nanometers in size. After the incorporation of ruthenium, the regular nanotube morphology

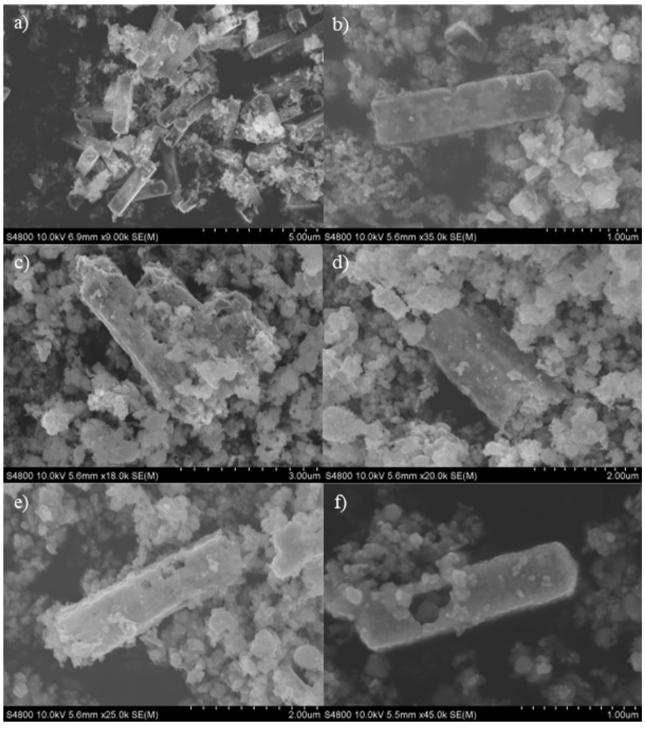

Figure 2. SEM images of the modified Co_3O_4 catalysts after calcination at 500 °C. (a) Co_3O_4, (b) $1Ru/Co_3O_4$, (c) Co_3O_4–F, (d) $0.5Ru/Co_3O_4$–F, (e) $0.75Ru/Co_3O_4$- F, and (f) $1Ru/Co_3O_4$–F.

https://doi.org/10.1021/acs.iecr.3c04045
Ind. Eng. Chem. Res. 2024, 63, 3003–3017

was partially lost probably due to sintering during the second calcination process (500 °C). Thus, a substantial number of nanoparticles (derived from the nanotube wall breakage) were found together with the nanotubes (Figure 2b). Nonetheless, no appreciable changes in the morphology were noticed after Ru impregnation.

It is widely accepted that the activity of metal oxide catalysts for oxidation reactions is mostly influenced by the abundance of highly mobile oxygen species. To further investigate the impact of the noble metal deposition on the reducibility of cobalt oxide, H_2-TPR experiments were conducted. The reduction profiles in the 50−500 °C temperature range of the Co_3O_4 and $1Ru/Co_3O_4$ samples are presented in Figure 3.

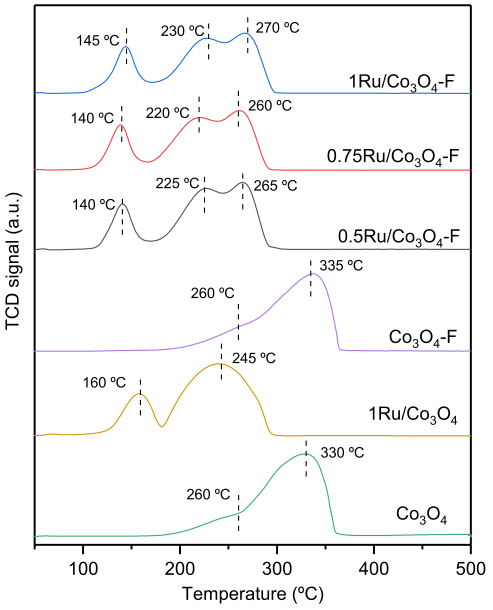

Figure 3. H_2-TPR profiles of the modified Co_3O_4 catalysts.

For the bare Co_3O_4 catalyst, two overlapping signals were distinguished between 200 and 360 °C, in agreement with a two-step reduction mechanism ($Co^{3+} \rightarrow Co^{2+} \rightarrow Co^0$).[26] After the incorporation of RuO_2 (as will be shown later by XPS), the reduction process shifted toward substantially lower temperatures. Thus, two distinct reduction peaks at 100−180 and 180−300 °C were observed. Recall that the total reduction of the blank cobalt oxide was attained over 360 °C. It could therefore be concluded that the deposition of Ru onto the spinel structure markedly promoted its reduction at lower temperatures. Some authors agree that the decrease in the reduction temperature of Ru-impregnated samples was due to the hydrogen spillover effect. Ru oxide was reduced at significantly lower temperatures (according to literature, between 100 and 175 °C[13,27]) in comparison with Co_3O_4. Then, the metallic ruthenium could act as a reduction nucleus and generate atomic hydrogen that spread to Co_3O_4 to accelerate its reduction.[11] In view of the shape of the reduction profile, it could be deduced that the process took place via the same two-step mechanism. Hence, Co_3O_4 was first reduced to CoO at about 160 °C and subsequently fully transformed into metallic Co at 245 °C. It must be pointed out that since the amount of Ru in the sample was very small, the H_2 uptake attributed to the reduction of ruthenium oxide was expected to overlap with the first reduction peak of Co_3O_4.

As a complementary technique to evaluate the mobility of surface and bulk oxygen species, O_2-TPD measurements were carried out in the 50−900 °C temperature range. Generally, surface oxygen species (both adsorbed and lattice species) are desorbed below 700 °C; meanwhile, bulk oxygen species need temperatures higher than 700 °C to desorb.[28] Figure 4

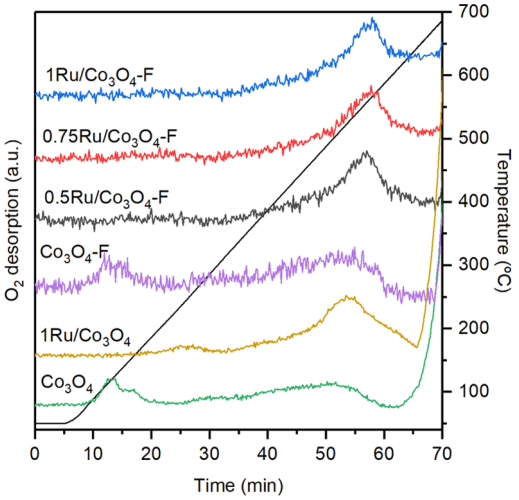

Figure 4. O_2-TPD profiles of the modified Co_3O_4 catalysts.

includes the O_2-TPD profiles of the bare and Ru-promoted Co_3O_4 catalysts. Note that the intense desorption signal above 700 °C that appeared over both samples due to thermal decomposition of Co_3O_4 is not shown. As regards surface oxygen species, several desorption peaks ascribed to oxygen species with varying nature could be distinguished. Thus, pure Co_3O_4 exhibited two overlapping desorption peaks between 120 and 150 °C, ascribed to surface-adsorbed oxygen species, which were not present in the promoted counterpart. Some authors state that Ru doping diminishes the amount of surface-adsorbed oxygen due to the formation of Ru−O−Co bond or partial blockage of pore structure by Ru species.[29] At higher temperatures, a weak desorption peak could be noticed at 245 and 290 °C for the $1Ru/Co_3O_4$ and Co_3O_4 samples, respectively. Finally, above 350 °C, a markedly intense desorption peak over the $1Ru/Co_3O_4$ catalyst could be identified, corresponding to the desorption of surface lattice oxygen species.[30] From the integration of the desorption profiles, it was found that the amount of desorbed oxygen species up to 700 °C increased from 41 μmol O_2 g^{-1} over the bare Co_3O_4 catalyst to 63 μmol O_2 g^{-1} over the Ru-containing sample (Table 1). In sum, results of H_2-TPR and O_2-TPD revealed a superior oxygen mobility and a higher amount of surface oxygen species in the $1Ru/Co_3O_4$ catalyst, features of high interest in chlorocarbon combustion.

XPS analysis was employed to further investigate the composition and chemical state of the surface of the synthesized samples since it is frequently claimed that the species at the surface play a critical role in oxidation reactions.[31] Figure 5 presents the Co $2p_{3/2}$, O 1s, and Ru $3p_{3/2}$ (for the $1Ru/Co_3O_4$ sample) XPS spectra of the as-prepared catalysts. The Co $2p_{3/2}$ signal could be deconvoluted into five peaks. The peak at 779.8 eV was related to surface Co^{3+} species in octahedral sites, whereas the signal at 780.8 eV was ascribed to surface Co^{2+} species in tetrahedral sites. The contribution at 781.9 eV was correlated to the presence of

https://doi.org/10.1021/acs.iecr.3c04045
Ind. Eng. Chem. Res. 2024, 63, 3003−3017

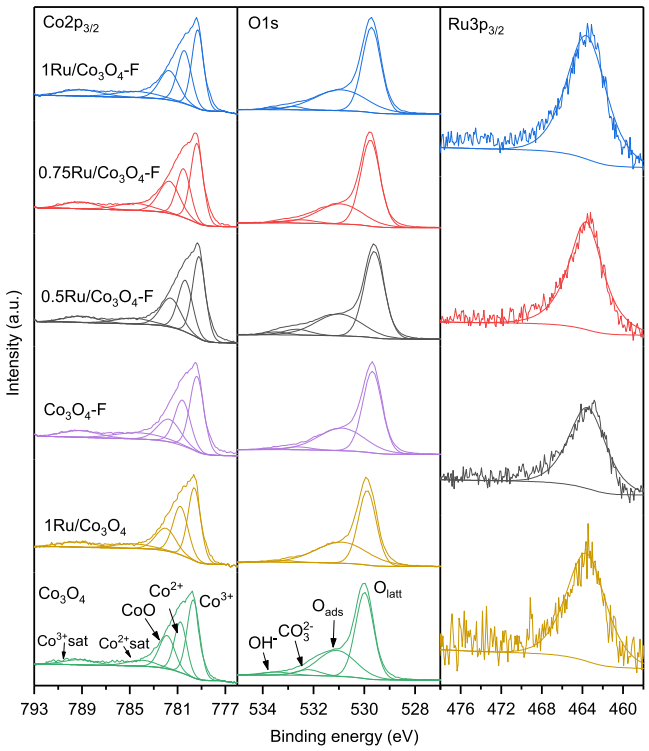

Figure 5. XPS profiles of the modified Co_3O_4 catalysts.

CoO species generated by reduction under vacuum conditions in the XPS chamber. For all samples, its abundance was lower than 20% of the total amount of cobalt. Finally, the lower intensity peaks at 783.8 and 789.5 eV were shakeup satellites of CoO and Co_3O_4, respectively.[32] On the other hand, the O 1s spectra were characterized by broad signals, which evidenced the presence of various oxygen species with different chemical states. Thus, the bands at 530.0 and 530.8 eV were ascribed to lattice and adsorbed oxygen species, while the signals at 531.9 and 532.9 eV were correlated to the presence of adsorbed carbonates and water, respectively.[33] On the Ru $3p_{3/2}$ spectra, only one signal centered at 463.6 eV could be observed, which was correlated to the Ru^{4+} cation.[12] No peaks associated with metallic Ru or other oxidation states of ruthenium were noticed, evidencing that the Ru species on the catalyst surface were essentially in the form of RuO_2. The amount of Ru in the $1Ru/Co_3O_4$ catalyst was estimated to be about 8 wt % with a surface Ru/Co molar ratio of 0.09, while the bulk Ru/Co molar ratio (calculated from EDX results) was 0.008, evidencing that the ruthenium species were mainly on the catalyst surface, without entering into the inner structure. The Co^{2+}/Co^{3+} and O_{ads}/O_{latt} molar ratios for the samples are shown in Table 2. As expected, the population of adsorbed oxygen species was controlled by a higher amount of cobalt in low oxidation state (Co^{2+}). Moreover, the Co^{2+}/Co^{3+} ratio appreciably increased after the addition of Ru, from 0.64 to 0.81. This observation suggested that the Ru species interacted with the Co_3O_4 surface causing the reduction of Co^{3+} species to Co^{2+} species. In the same line, the O_{ads}/O_{latt} ratio increased from 0.63 for bare Co_3O_4 to 0.81 after Ru incorporation. This increase in surface oxygen vacancies (also confirmed by H_2-TPR and O_2-TPD) was due to the formation of the Ru−O−Co bond, which caused disorder in the Co_3O_4 lattice and favored the creation of structural defects.[12] Moreover, the electrons flow from Ru atoms to Co atoms through the Ru−O−Co bond provoked a rise in the surface Co^{2+} species. This assumption was also confirmed by the slight shift toward lower binding energy (~0.1 eV) of the Co $2p_{3/2}$ signal after the incorporation of Ru.[34,35]

Table 2. Surface Composition of the Modified Co_3O_4 Catalysts

catalyst	Co^{2+}/Co^{3+} molar ratio	O_{ads}/O_{latt} molar ratio	Ru^{4+}, wt %	Ru/Co molar ratio
Co_3O_4	0.64	0.63		
$1Ru/Co_3O_4$	0.81	0.81	8	0.09
Co_3O_4−F	0.67	0.66		
$0.5Ru/Co_3O_4$−F	0.75	0.71	6	0.09
$0.75Ru/Co_3O_4$−F	0.70	0.67	9	0.11
$1Ru/Co_3O_4$−F	0.79	0.77	10	0.12

3.2. Catalytic Behavior of Co_3O_4 and $1Ru/Co_3O_4$ Catalysts. The catalytic efficiency for the oxidation of 1,2-DCE was evaluated by following the conversion to CO_2 with temperature. 1,2-DCE was chosen as a model for the category of double carbon chlorinated VOCs with a H/Cl ratio of >1. This compound typically exhibits an intermediate ease of oxidation between single-chlorinated double carbon olefins such as vinyl chloride[36] and polychlorinated olefins such as dichloroethylene and trichloroethylene.[37] Figure 6 shows the

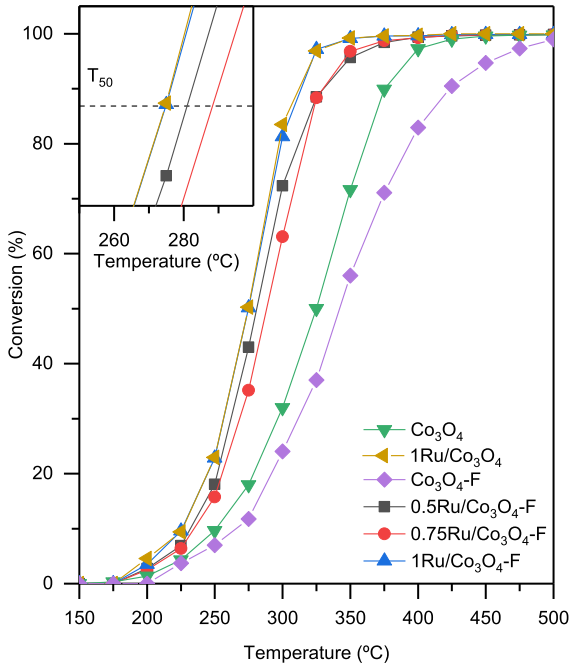

Figure 6. Light-off curves of the modified Co_3O_4 catalysts.

light-off curves between 150 and 500 °C at 15,000 h^{-1}. The corresponding values of T_{50} and T_{90} (temperatures needed to attain 50 and 90% conversion to CO_2, respectively) are included in Table 3.

Pure Co_3O_4 exhibited a reasonably good performance with T_{50} and T_{90} values of 325 and 375 °C, respectively. After the addition of ruthenium, the light-off curve shifted to lower temperatures, leading to the complete oxidation of the pollutant at 310 °C. Therefore, it could be deduced that the incorporation of low amounts of ruthenium introduced beneficial changes essentially related to promotion of oxygen

https://doi.org/10.1021/acs.iecr.3c04045
Ind. Eng. Chem. Res. 2024, 63, 3003−3017

Table 3. Kinetic Results of the Oxidation of DCE over the Modified Co_3O_4 Catalysts[a]

catalyst	T_{50}, °C	T_{90}, °C	$(-r_A)$, mmol g^{-1} h^{-1}	E_a, kJ mol^{-1}	$\ln(k_0)$[d]
Co_3O_4	325	375	0.29[b]	70 ± 1.3	8.3 ± 0.3
$1Ru/Co_3O_4$	275(280)	310(340)	0.36[c]	92 ± 2.4	14.4 ± 0.6
Co_3O_4−F	340	420	0.18[b]	66 ± 1.8	7.0 ± 0.4
$0.5Ru/Co_3O_4$−F	280	330	0.28[c]	86 ± 3.8	12.8 ± 0.8
$0.75Ru/Co_3O_4$−F	290	330	0.25[c]	87 ± 0.6	12.7 ± 0.1
$1Ru/Co_3O_4$−F	275	310	0.36[c]	89 ± 1.9	13.8 ± 0.4

[a]Results in parentheses corresponded to the second reaction cycle. [b]Calculated at 275 °C. [c]Calculated at 250 °C. [d]k_0 is expressed as mol g^{-1} s^{-1} MPa^{-1}.

mobility or oxygen vacancies of the spinel that eventually would result in an increased oxidation activity. To verify that the $1Ru/Co_3O_4$ catalyst is not only active but also stable, a consecutive light-off run was carried out (Figure S2, Supporting Information). The temperature to reach the total oxidation of DCE increased by 30 °C, thus pointing out a significant deactivation of the sample after the first reaction cycle. This loss of activity could be due to the volatilization of a certain amount of RuO_2 species from the surface of the catalyst. In this sense, EDX analysis of the used sample (submitted to two consecutive light-off tests) revealed a slight decrease in the Ru content from 1 to 0.9 wt %. Similarly, XPS results evidenced a much more marked loss of surface Ru (by 30%), from 8 to 5 wt %. Accordingly, the surface Ru/Co molar ratio dropped from 0.09 to 0.05.

As stated previously, the stability of noble metal-modified transition-metal oxide catalysts can be enhanced by strengthening the interaction between the promoter and the bulk oxide. In this sense, acid-etching is a widely employed approach to improve the anchoring of metal particles.[38] Thus, in an attempt to obtain highly active and stable Ru/Co_3O_4 catalysts for the oxidation of chlorinated compounds, the freshly prepared cobalt oxide was treated with an aqueous HF solution (1.2 M) to upgrade metal−support interactions. Then, Ru species were impregnated on the modified oxide. The effect of HF etching on the physical-chemical properties of the Co_3O_4 active phase was extensively examined, and the main results will be discussed below.

3.3. Structural Changes of Co_3O_4 after HF-Etching and Catalytic Behavior. First, the effect of acid treatment on the textural properties of the parent cobalt oxide was studied. Similar to the fresh Co_3O_4 sample, the acid-etched counterpart exhibited a type IV isotherm with H1 hysteresis loop, which suggested that the characteristic mesopore structure was maintained after the acid treatment (Figure S1, Supporting Information). However, a significant loss of specific surface area and pore volume was observed (Table 1). On the other hand, the X-ray diffractogram (Figure 1) of the Co_3O_4−F sample displayed the same diffraction signals attributable to the spinel structure (ICDD 00-042-1467). Thus, the HF etching did not provoke the structural collapse of the spinel lattice. Nevertheless, an appreciable increase in crystallite size (from 22 to 35 nm) was noticed. This observation was also found by Li et al., who reported a strengthening in the crystallinity of Mn_3O_4−Fe_2O_3 after treating the mixed oxides with hydrochloric acid.[39] To gain further insights into the structure of the cobalt oxide, both fresh and etched samples were additionally examined by Raman spectroscopy as well. Hence, the spectra include five Raman bands (A_{1g} + E_g + $3F_{2g}$) in the 100−800 cm^{-1} range (Figure S3, Supporting Information). After the acid modification, an increase in the full width at half-maximum of the A_{1g} vibration mode was observed, in line with the formation of a highly defective structure.[40]

The influence of the acid treatment on the morphology of the nanotubes was evaluated by SEM. From the inspection of Figure 2a,c, it could be deduced that after HF-etching, the hollow morphology was almost completely destroyed leading to the aggregation of nanoparticles of irregular size. However, the walls of the remaining nanotubes were distinctly rough, which could be due to the generation of surface defects during the acid treatment. In view of the textural and structural results, it could be stated that HF induced an increase in the structural disorder of the Co_3O_4 phase.

The bulk oxygen mobility of the acid etched-Co_3O_4 was also evaluated by means of H_2-TPR and O_2-TPD (both bulk and surface) analyses. The results are shown in Table 1 and Figures 3 and 4. Similar to the bare Co_3O_4 sample, the acid-etched counterpart showed the characteristic two-step reduction mechanism. The temperatures of the reduction peaks hardly varied with respect to the untreated sample (260 and 335 °C, respectively). As for the O_2-TPD analysis, comparable results were also found for both Co_3O_4 samples. Two overlapping desorption peaks between 120 and 150 °C (surface-adsorbed oxygen species) and a weaker signal above 350 °C ascribed to surface lattice oxygen species were noticed. Regarding the total quantity of oxygen species, both samples evidenced very similar amounts (41 μmol O_2 g^{-1} over the fresh Co_3O_4, and 40 μmol O_2 g^{-1} over the modified counterpart). These results pointed out that the amount and mobility of bulk oxygen species barely changed after the acid modification. However, it would be of interest to closely examine the effects of acid modification on the surface of the oxide.

To confirm the generation of defects on the surface, XPS analysis of the Co_3O_4−F sample was performed. Following the same procedure described earlier for identification and assignment of deconvoluted signals, the corresponding Co $2p_{3/2}$ and O 1s XPS spectra are displayed in Figure 5. Interestingly, significantly higher surface Co^{2+}/Co^{3+} (0.67) and O_{ads}/O_{latt} (0.66) molar ratios were obtained in comparison with those found over the untreated oxide (0.64 and 0.63, respectively), thereby confirming the generation of surface defects by the acid treatment in consistency with both Raman and SEM results. XPS analysis was also useful for determining the eventual accumulation of fluorine atoms on the surface. Judging from the absence of the signal at 686 eV of the F 1s spectrum, it was thus confirmed that these species were not present.

The acid-etched cobalt oxide was catalytically evaluated for the oxidation of DCE. The obtained light-off curve as well as the T_{50} and T_{90} values are included in Figure 6 and Table 3, respectively. After acid treatment, the T_{50} value increased by 15 °C compared with the untreated cobalt oxide. This decrease in

https://doi.org/10.1021/acs.iecr.3c04045
Ind. Eng. Chem. Res. 2024, 63, 3003−3017

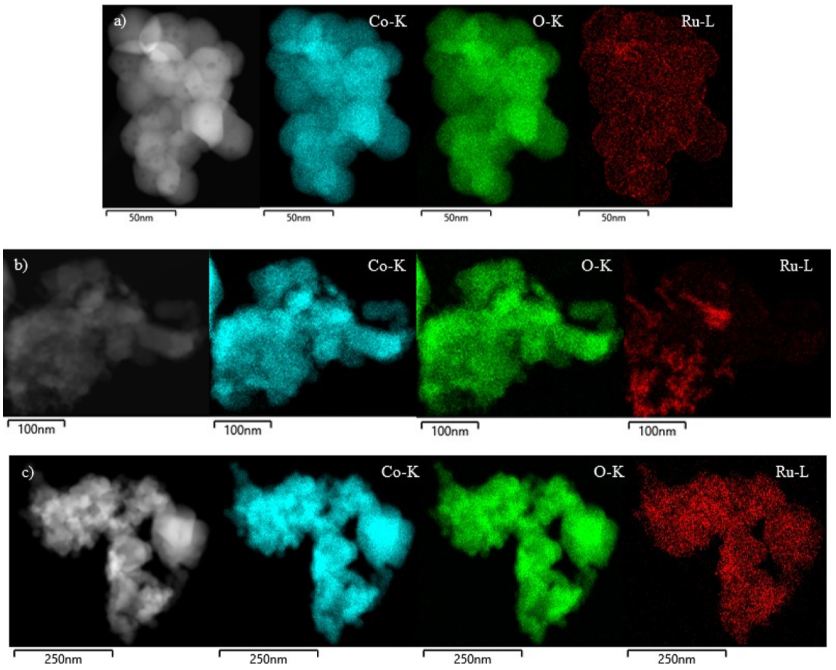

Figure 7. STEM-HAADF images and SEM−EDX maps of the modified Co_3O_4 catalysts: (a) 0.5Ru/Co_3O_4−F, (b) 0.75Ru/Co_3O_4−F, and (c) 1Ru/Co_3O_4−F. (Blue) cobalt, (green) oxygen, and (red) ruthenium.

activity was also observed when comparing the reaction rate results (under differential conditions) given by the untreated sample (0.29 mmol g^{-1} h^{-1}) and the HF-etched sample (0.18 mmol g^{-1} h^{-1}). This loss of the catalytic efficiency revealed that the generation of surface defects, induced by the acid treatment, was not enough to make up for the observed decrease in surface area and the enlargement of the Co_3O_4 crystallite size. In any case, it should be kept in mind that the main target of the acid treatment of the cobalt oxide was not to obtain an active catalyst in the oxidation of chlorinated compounds, but the generation of structural and surface defects that tentatively may enhance ruthenium dispersion and favor metal−support interaction, thus resulting in remarkably active and stable Ru/Co_3O_4 catalysts.

Once the highly defective HF-modified Co_3O_4 was prepared, ruthenium was deposited following an impregnation method. To study the influence of the amount of Ru, three catalysts with different loadings, namely, 0.5, 0.75, and 1 wt %, were prepared. The *x*Ru/Co_3O_4−F catalysts were thoroughly characterized and evaluated in the oxidation of DCE.

3.4. Physical-Chemical Characterization of the *x*Ru/Co_3O_4−F Catalysts. After the incorporation of the ruthenium as RuO_2, the resulting catalysts preserved their textural properties. The specific surface area of the solids slightly increased with respect to that of Co_3O_4−F, although no noticeable differences were noted with the Ru loading. Type IV isotherms with H1 hysteresis cycles were also observed (Figure S1, Supporting Information), which suggested that the mesoporous structure was mostly retained upon ruthenium impregnation. Results of BET surface area, pore volume, and mean pore diameter (Table 1) were quite similar for all the Ru-impregnated catalysts, namely, a surface area of around 10 m^2 g^{-1}, a pore volume between 0.02 and 0.03 cm^3 g^{-1}, and a mean pore diameter of about 180−200 Å.

The XRD patterns presented in Figure 1 obviously showed the set of diffraction peaks corresponding to the cubic spinel Co_3O_4 oxide, at 2θ = 19.2, 31.4, 37.0, 38.7, 45.0, 55.8, 59.5, and 65.4°. In line with the results for the 1Ru/Co_3O_4 sample, no diffraction peaks corresponding to metallic ruthenium or ruthenium oxides were detected, owing to the low concentration and high dispersion of the promoter. All the catalysts exhibited similar values of Co_3O_4 crystallite size between 36 and 37 nm (Table 1). Complementarily, the samples were characterized by STEM-HAADF. The corresponding particle size distribution histograms are presented in Figure S4, Supporting Information. The average particle size was calculated from the measurement of a set of particles, typically larger than 150 and never below 100. The obtained values ranged between 31 and 34 nm (Table 1), in fairly good agreement with XRD results. As regards the particle size distribution, it should be pointed out that between 75 and 80% of the particles were smaller than 35 nm for all the catalysts.

The SEM images of the *x*Ru/Co_3O_4−F catalysts are shown in Figure 2d−f. A heterogeneous morphology could be found for all the samples, as a mixture of nanotubes and irregular clusters formed by the agglomeration of discrete nanoparticles. On the other hand, when comparing the external morphology of the Ru-modified samples with that of the fresh and acid-etched Co_3O_4, several differences could be seen. The walls of the 1Ru/Co_3O_4 sample (Figure 2b) were quite smooth. However, the 1Ru/Co_3O_4−F catalyst (Figure 2f) exhibited rougher walls, which could be an indication of surface defects.

To gain more insights into the dispersion of the Ru species on the surface of the modified cobalt oxide, EDX-mapping images were taken (Figure 7). As far as the 0.5Ru/Co_3O_4−F catalyst was concerned, it was observed that ruthenium was homogeneously distributed over the entire surface of the support. As the Ru loading increased (0.75%), this distribution became more heterogeneous since regions with markedly variable Ru density were noted. On the other hand, when increasing the Ru loading up to 1%, a more homogeneous distribution was also observed although with a higher density than that in the 0.5Ru/Co_3O_4−F sample. These findings

https://doi.org/10.1021/acs.iecr.3c04045
Ind. Eng. Chem. Res. 2024, 63, 3003−3017

evidenced that the HF etching favored the dispersion of RuO_x species.

The corresponding H_2-TPR profiles of the catalysts are displayed in Figure 3. The xRu/Co_3O_4−F samples exhibited two well discernible uptakes at 100−180 °C and 180−300 °C assignable to the reduction of Co^{3+} to Co^{2+} and finally to Co^0. The low-temperature peak was around 140−145 °C, somewhat lower (15 °C) than that over the 1Ru/Co_3O_4 catalyst. Besides, a significant distortion in the high-temperature uptake over the acid-etched catalysts was observed. Nevertheless, the total reduction of the xRu/Co_3O_4−F and the 1Ru/Co_3O_4 samples was fulfilled at the same temperature (300 °C). It was found that, within the experimental error, the observed uptakes (16.8−17.0 mmol H_2 g^{-1}) coincided with the theoretical consumption (16.6 mmol H_2 g^{-1}). Moreover, no obvious differences in the reduction temperatures could be detected as a function of Ru content. According to literature, with promoter loadings above a certain amount, the maxima of the peak reduction temperatures are not affected, and there is no further promotion due to the partial accumulation of ruthenium oxide on the surface of Co_3O_4.[41]

Figure 4 includes the O_2-TPD profiles for the Ru-promoted catalysts. The three samples exhibited a similar desorption profile, with a peak temperature around 550 °C. The amounts of desorbed surface oxygen species were estimated by integrating the areas of the desorption signal below 700 °C (Table 1) and decreased as follows: 1Ru/Co_3O_4−F (60 μmol g^{-1}) > 0.5Ru/Co_3O_4−F (52 μmol g^{-1}) > 0.75Ru/Co_3O_4−F (49 μmol g^{-1}). These results suggested that the oxygen mobility was considerably promoted over the 1Ru/Co_3O_4−F sample (very similar to that of the 1Ru/Co_3O_4 catalyst, 63 μmol g^{-1}) followed by the 0.5Ru/Co_3O_4−F and 0.75Ru/Co_3O_4−F oxides.

Finally, the surface composition and chemical state of the as-prepared catalysts were analyzed by XPS. The Co $2p_{3/2}$, O 1s, and Ru $3p_{3/2}$ XPS spectra are shown in Figure 5. The signals were deconvoluted according to the procedure explained before. It must be highlighted that again only Ru^{4+} species were detected over the various xRu/Co_3O_4−F catalysts. The Co^{2+}/Co^{3+} and O_{ads}/O_{latt} molar ratios as well as the surface Ru^{4+} content over the samples are shown in Table 2. It was found that the 1Ru/Co_3O_4−F catalyst exhibited the highest Co^{2+}/Co^{3+} and O_{ads}/O_{latt} molar ratios on the surface followed by the 0.5Ru/Co_3O_4−F sample, which was expected to be beneficial for Cl-VOC oxidation. Conversely, the 0.75Ru/Co_3O_4−F catalyst showed the lowest molar ratios. As previously stated, after the incorporation of ruthenium, the amount of oxygen vacancies as well as the population of Co^{2+} species increased owing to the electrons flow from Ru atoms to Co atoms through the Ru−O−Co bond. This assumption was further corroborated by Raman analysis. After the ruthenium addition, the A_{1g} vibration mode of Co−O red-shifted (Figure S5, Supporting Information), which suggested that the RuO_2 can sway the stretching vibration of Co−O bond, implying the creation of Ru−O−Co bonds.[42] On the other hand, the amount of surface Ru was higher in the 1Ru/Co_3O_4−F sample (10 wt %) than that in the 1Ru/Co_3O_4 catalyst (8 wt %), which pointed out that the acid treatment favored the dispersion of the Ru species on the surface of the catalyst.

3.5. Catalytic Behavior of the xRu/Co_3O_4−F Catalysts.

The behavior of the xRu/Co_3O_4−F catalysts for DCE oxidation to CO_2 as a function of temperature is shown in Figure 6. Besides, the corresponding values of T_{50} and T_{90} (temperatures needed to attain 50 and 90% conversion, respectively) are listed in Table 3. The modified cobalt catalysts showed an excellent performance since in all cases, the chlorinated ethane was fully oxidized to CO_2 (>90% conversion) below 330 °C. Moreover, after the incorporation of ruthenium oxide, the catalytic efficiency of the samples was appreciably boosted since the T_{50} values decreased by 50−65 °C in comparison with the Co_3O_4−F sample.

Judging from the catalytic results presented in Table 3, significant differences in the catalytic performance were noticed as a function of the amount of ruthenium. The temperature required for 50% conversion was in the 275−290 °C range; meanwhile, 90% conversion was achieved between 310 and 330 °C. By considering the T_{50} value, the catalytic efficiency of the Ru-promoted cobalt oxide catalysts ranked as follows: 1Ru/Co_3O_4−F > 0.5Ru/Co_3O_4−F > 0.75Ru/Co_3O_4−F. On the other hand, the used samples were characterized by EDX and TPO to evaluate the chlorination of the catalysts as well as the formation of carbonaceous deposits. EDX analysis revealed the presence of small amounts of chlorine (0.15−0.20 wt %) on the samples. On the other hand, TPO measurements coupled to mass spectrometry revealed that the coke generation during the reaction was negligible. Thus, when increasing the temperature with a heating ramp of 10 °C min^{-1} under a controlled atmosphere (5%O_2/He) up to 800 °C, a mass loss associated with water desorption (m/z = 18) was detected at around 100 °C. However, at higher temperatures, no noticeable mass change was observed. Accordingly, the profile of the CO_2 signal (m/z = 44), which could be formed because of the combustion of the eventually formed carbonaceous deposits, in the corresponding mass spectrum was flat. These findings were also consistent with the C balance, which was around 100% (within the experimental error) throughout the whole reaction run.

The intrinsic activity of the samples was better assessed in terms of the measured reaction rate under differential conditions at 250 °C (when conversion was below 20%). The results presented in Table 3 exhibit the same trend as that dictated by the T_{50} values. The 1Ru/Co_3O_4−F sample showed the highest reaction rate (0.36 $mmol_{DCE}$ g^{-1} h^{-1}) followed by the 0.5Ru/Co_3O_4−F and 0.75Ru/Co_3O_4−F samples (0.28 and 0.25 $mmol_{DCE}$ g^{-1} h^{-1}, respectively). Figure 8 reveals a reasonable correlation among the intrinsic reaction rate, the amount of surface active oxygen species (as estimated by O_2-TPD analysis and by XPS), and the surface Co^{2+}/Co^{3+} molar ratio (as determined by XPS). The results corresponding to the 1Ru/Co_3O_4 catalyst were also included. As previously stated, the incorporation of Ru species onto the surface of the Co_3O_4 provoked the reduction of Co^{3+} species increasing the amount of surface Co^{2+}, which in turn was related to oxygen defects close to the surface. Hence, the promotion of oxygen vacancies can activate gas-phase oxygen molecules to generate active oxygen species.

These correlations between activity and physicochemical properties were better rationalized when the mechanism of catalytic oxidation reactions of chlorinated VOCs over the cobalt catalyst was taken into account. According to literature, first, chlorinated molecules adsorb on Co^{2+} sites. Then, the adsorbed molecule is attacked by the active oxygen species on the surface of the catalyst, which are responsible for breaking the C−Cl bond. Thus, the Cl species fill the oxygen vacancy on the catalyst surface. Finally, Ru species facilitate the release of Cl species via the Deacon reaction, and active oxygen species

https://doi.org/10.1021/acs.iecr.3c04045
Ind. Eng. Chem. Res. 2024, 63, 3003−3017

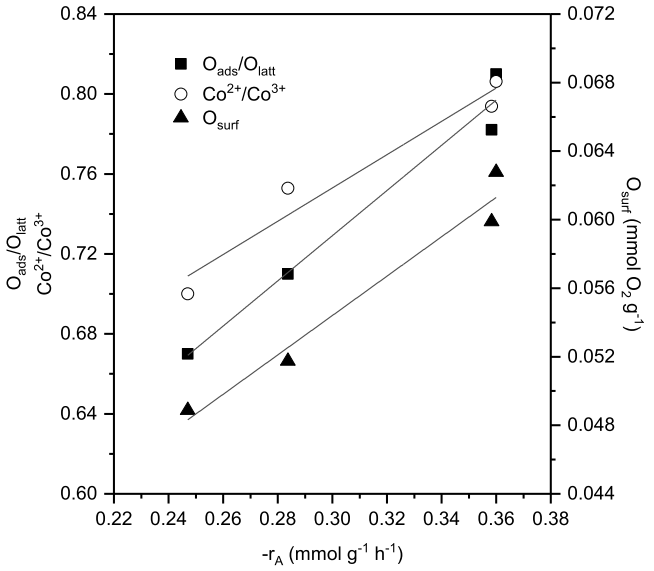

Figure 8. Relationship among the specific reaction rate, the amount of active oxygen species, and the Co^{2+}/Co^{3+} and O_{ads}/O_{latt} molar ratios.

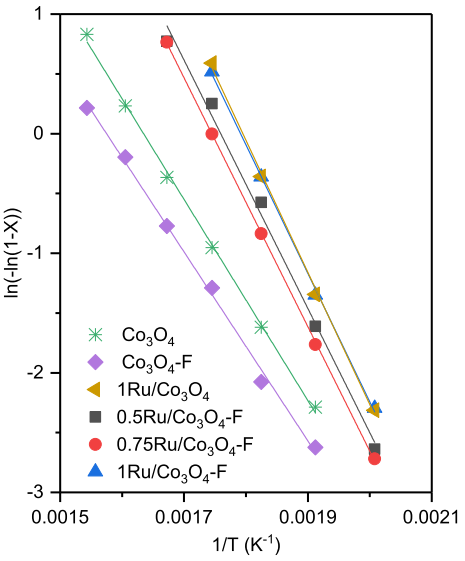

Figure 9. Pseudo-first-order fit for the experimental data obtained over the modified Co_3O_4 catalysts.

on the catalyst surface play a crucial role in fully converting adsorbed hydrocarbon species into CO_2.[15] As demonstrated previously, the population of Co^{2+} and O_{ads} species increased after Ru incorporation, which was favorable for DCE oxidation since the surface Co^{2+} sites were the active sites for DCE adsorption, and O_{ads} species were the responsible for the oxidation of the chlorinated VOC to CO_2.

Kinetic studies were accomplished considering pseudo-first-order kinetics in DCE, zero order for oxygen (owing to its large concentration), and an Arrhenius dependence of the rate constant. These kinetic models are frequently reported in the literature for Cl-VOC oxidation and used for catalyst comparison and preliminary reactor design.[9,43] These conditions were assumed to be valid for the catalytic oxidation of DCE in chlorinated VOC-air diluted mixtures over the examined Ru-promoted cobalt catalysts. To determine the kinetic parameters (i.e., activation energy and pre-exponential factor), the integral method (conversion between 5 and 80%) was applied. Consequently, if the change in density of the reactant gas due to reaction is considered negligible (since DCE is very diluted), then the following linearized equation can be derived for the integral reactor

$$\ln[-\ln(1-X)] = \ln[(k_0 P_{DCE_0}(W/F_{DCE_0})] - E_a/RT \quad (1)$$

where X is the fractional conversion of DCE, k_0 is the pre-exponential factor of the Arrhenius equation, and $W/F_{DCE,0}$ is the w8 hly space velocity. Pre-exponential factor and apparent activation energies estimated from eq 1 are included in Table 3. In Figure 9, the goodness of the numerical fit for the kinetic study is shown. The obtained values for the activation energy were in the 86−92 kJ mol^{-1} range for the Ru-promoted catalysts and about 70 kJ mol^{-1} for the parent cobalt oxides, quite similar for all the samples, which evidenced that the reaction mechanism was the same irrespective of the investigated catalyst. These E_a values were comparable with those reported in the literature for the combustion of chlorinated VOCs over Co_3O_4 and Ru-promoted Co_3O_4 catalysts[6,44−47] (Table 4). Since all the catalysts exhibited a relatively comparable value of the apparent activation energy, the ratio between the values of the pre-exponential factor was taken as an indication of the relative activity of the studied oxides. Thus, it was observed that 1Ru/Co_3O_4−F was about three times more active than 0.75Ru/Co_3O_4−F and about 2.7 times more active than 0.5Ru/Co_3O_4−F. These results corroborate the trend derived from the light-off curves and the specific reaction rate. On the other hand, theoretical conversion values could be estimated from the kinetic model and compared with those obtained experimentally. Figure S6, Supporting Information shows a good relationship between the experimental and theoretical conversion values, which validated the proposed kinetic rate expression over the studied temperature range.

The catalysts examined in this study introduce research path on catalytic systems that could be used in oxidation reactions. Although a large number of studies on Ru−Co_3O_4 systems for the oxidation of volatile organic compounds with varying chemical nature (both chlorinated and nonchlorinated hydrocarbons) can be found in the literature, very few of them deal with the acid modification of the cobalt spinel to improve the activity and stability of the resultant catalysts. Instead, most of these investigations focus on the variation of the noble metal loading (0.5−1% wt), studying various routes of cobalt oxide synthesis (impregnation, precipitation, and sol−gel), or the use of supports with high-surface area (ZIF-67, titania, or alumina nanosheets).[11,12,15,29,48−50] This is why we consider that our results can be a very interesting starting point in the development of new strategies for obtaining efficient cobalt catalysts for the oxidation of recalcitrant pollutants. A comparative analysis of similar catalytic systems found in the literature is shown in Table 5. Hence, it was found that Ru−Co_3O_4-based catalysts, when operating at relatively high WHSV, are adequate candidates for the removal of light hydrocarbons, aromatic compounds, and chlorocarbons, with oxidation temperatures for full conversion lower than around 300 °C.

The product distribution of the synthesized catalysts as a function of temperature was also examined. For the Ru-free cobalt oxide catalysts, the main chlorinated byproducts detected were chlorinated methanes (dichloromethane, trichloromethane, and tetrachloromethane) and, to a lesser

https://doi.org/10.1021/acs.iecr.3c04045
Ind. Eng. Chem. Res. 2024, 63, 3003−3017

Table 4. Comparison of the Activation Energies in Chlorinated VOC Oxidation with Cobalt Oxide Catalysts Reported in the Literature

catalyst	chlorinated VOC	Cl-VOC concentration, ppm	WHSV, mL g^{-1} h^{-1}	E_a, kJ mol^{-1}	reference
xRu/Co_3O_4−F	DCE	1000	35,000	86−89	this work
Co_3O_4-7P	DCM	3000	60,000	107	6
ZIF-Co	VC	1000	15,000	101	44
Co_3O_4	CB	1000	60,000	71	45
Co_3O_4	VC	1000	15,000	76−84	46
RuO_x/Co_3O_4−IM	DCE	1000	60,000	96	47

Table 5. Catalytic Performance of Ru−Co_3O_4 Catalysts in the Oxidation of VOCs

catalyst	chlorinated VOC	Cl-VOC concentration, ppm	WHSV, mL g^{-1} h^{-1}	T_{90}, °C	reference
1Ru/Co_3O_4−F	DCE	1000	35,000	310	this work
0.5Ru/Co_3O_4−F	DCE	1000	35,000	330	this work
1Ru/Co_3O_4	VC	1000	12,000	215	11
1Ru/Co_3O_4	DCB	1000	30,000	300	12
0.5Ru/Co_3O_4-10F	VC	20,000	30,000	250	15
0.5Ru/Co_3O_4	DCE	1000	45,000	330	29
1Ru-5Co/TiO_2	benzene	500	60,000	215	48
1Ru/Co_3O_4-MOF	toluene	1000	60,000	240	49
1Ru/CoANS	propane	1000	15,000	260 (T_{50})	50

extent, chlorinated ethylenes such vinyl chloride and *cis*-1,2-dichloroethylene. After the addition of ruthenium (Figure 10),

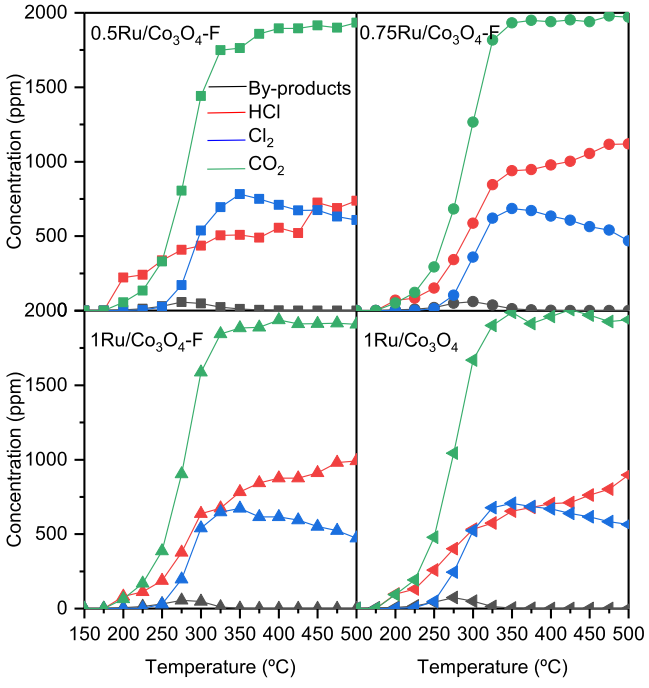

Figure 10. Product distribution during the catalytic oxidation of DCE over the modified Co_3O_4 catalysts.

these chlorinated hydrocarbons were also detected [dichloromethane (35−50 ppm), trichloromethane (15−20 ppm), and *cis*-1,2-dichloroethylene and tetrachloromethane (<5 ppm)]. However, their concentration was dramatically decreased. Interestingly, vinyl chloride, which is a known byproduct formed by dehydrochlorination of the feed, was not detected in any case, possibly due to the strong redox ability of the modified catalysts.[51] Besides, when comparing the product distribution over the two studied 1% Ru supported catalysts (1Ru/Co_3O_4 and 1Ru/Co_3O_4−F) (Figure 11), it was observed

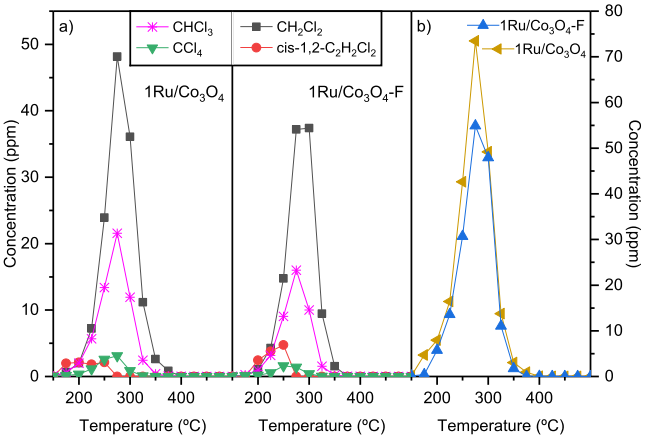

Figure 11. Comparison of the byproducts generated over the 1Ru/Co_3O_4 and 1Ru/Co_3O_4−F catalysts. (a) Byproducts chemical nature, (b) accumulated byproducts.

that the generation of byproducts was minimized over the whole temperature range studied when the HF-etched Co_3O_4 was used. These results highlighted the beneficial role of acid treatment in product selectivity. As aforementioned, HF-treatment improved the dispersion and increased the amount of Ru species on the Co_3O_4 surface. These Ru ions were responsible for removing the Cl species from the catalyst surface through the Deacon reaction. Thus, a higher concentration of Ru species could activate the desorption of Cl species from the catalyst surface and lead to a lower polychlorinated byproduct generation. On the other hand, the main chlorinated deep oxidation products were Cl_2 and HCl. Under complete DCE conversion conditions (325 °C), the observed Cl_2/HCl ratio was in the 1−1.4 range, except for the 0.75Ru/Co_3O_4−F sample, which exhibited a significantly lower value (0.7). These values were appreciably higher than that obtained for bare Co_3O_4 (0.7), attributable to the high activity of ruthenium oxide in the Deacon reaction.[13] It is worth highlighting that no CO was detected over the whole

https://doi.org/10.1021/acs.iecr.3c04045
Ind. Eng. Chem. Res. 2024, 63, 3003−3017

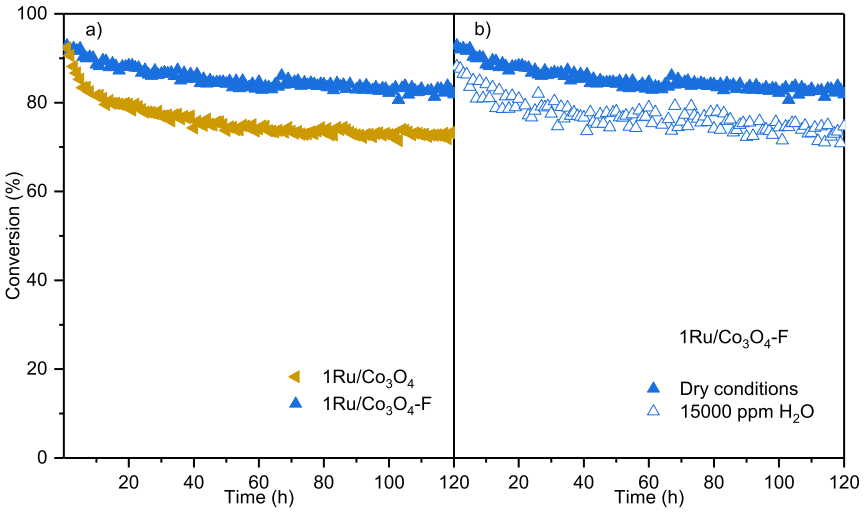

Figure 12. Stability in DCE oxidation at 300 °C for 120 h. (a) Comparison between $1Ru/Co_3O_4$ and $1Ru/Co_3O_4$−F samples, (b) $1Ru/Co_3O_4$−F under dry and humid conditions.

temperature range, and CO_2 was the main nonchlorinated oxidation product.

Finally, the catalytic stability of the most efficient promoted-oxide, namely, the $1Ru/Co_3O_4$−F catalyst, was investigated by analyzing the evolution of conversion to CO_2 with time on stream at 300 °C for 120 h (Figure 12). This run evidenced that conversion slightly decreased (about 10%) during the first 40 h. However, during the remaining 80 h, it remained stable (83%). The used $1Ru/Co_3O_4$−F sample was characterized by XRD, EDX, N_2 physisorption, and XPS. The crystallite size slightly enlarged from 36 nm on the fresh catalyst to 37 nm on the used sample. Interestingly, no diffraction peaks corresponding to the formation of less active species such as CoO or $RuCl_2$ were observed. In terms of textural properties, the stability test did not affect the surface area, which remained unaltered at 10 $m^2\ g^{-1}$. Finally, in view of the results shown in Figure 12, it could be expected that this relatively long stability test did not provoke a massive volatilization of the RuO_2 species. However, to confirm this assumption, EDX analysis was carried out on the used sample. The Ru content hardly changed after the 120 h test (both fresh and used samples showed a ruthenium content of about 0.9 wt %). Consequently, it was reasonable to conclude that the surface disorder induced by the acid-etching of the cobalt oxide improved the anchorage of Ru particles on the oxide and ultimately the stability of the catalyst. Likewise, the presence of small amounts of chlorine (0.25 wt %) was evidenced. However, it must be pointed out that the concentration of chlorine on the surface of the catalyst was noticeably higher (5.4 wt %) than that in the bulk. This accumulation of chlorine was probably responsible for the slight loss of activity during the first hours of the stability test. In fact, when the chlorine concentration in the sample after 20 h of reaction and at the end of the stability test (120 h) was compared, this hardly increased (4.5 and 5.4 wt %, respectively). In addition, similar results were found for the Cl/Ru molar ratio (about 1.9).

The good stability of this sample was best assessed when comparing it with the catalytic performance shown by its untreated counterpart ($1Ru/Co_3O_4$) under the same reaction conditions (Figure 12a). The results revealed that although both samples exhibited the same initial conversion value (~92%), the $1Ru/Co_3O_4$ sample underwent a more severe deactivation over time until it stabilized at around 73% conversion. This value was significantly lower than that shown by the $1Ru/Co_3O_4$−F sample (83%). Therefore, it could be concluded that the acid treatment of the cobalt oxide improved the thermal stability of the Ru species due to a stronger interaction between Co_3O_4 and RuO_2 species, which led to a better stability of the $1Ru/Co_3O_4$−F catalyst when operating during prolonged reaction time intervals.

The durability of this sample (120 h) was also evaluated at 300 °C under humid conditions (15,000 ppm of H_2O) (Figure 12b). After a slightly progressive decrease in conversion during the first 40 h, then it remained constant at 75%. This conversion value was somewhat lower than that obtained at the same temperature under dry conditions (83%), possibly due to the competitive adsorption of DCE and H_2O molecules.[52] Indeed, the surface chlorination of the catalysts under humid conditions was appreciably lower (2.0 wt %) owing to efficient role of H_2O in cleaning the catalyst surface. These results, however, indicated that the optimal $1Ru/Co_3O_4$−F catalyst exhibited both good catalytic stability and H_2O resistance in the catalytic oxidation of DCE at low temperatures. As for Cl_2/HCl selectivity, the formation of hydrogen chloride at the expense of molecular chlorine was substantially favored in the presence of excess water as the Cl_2/HCl molar ratio decreased from 0.8 under dry conditions to 0.5 under humid conditions. Moreover, the byproduct generation was dramatically diminished after the addition of water. Only 30 ppm of dichloromethane was detected after the addition of water; meanwhile, its concentration was about 110 ppm under dry conditions. Besides, the formation of trichloromethane was reduced from 30 to 10 ppm under humid conditions, and the generation tetrachloromethane was totally suppressed. This reduction in the byproduct yields could be explained by the inhibition of the reactivity of Cl_2 by water molecules as a hydrogen source.[53]

4. CONCLUSIONS

A series of Ru-promoted (with different Ru loadings) cobalt oxide catalysts with controlled nanomorphology were synthesized by a precipitation route based on the Kirkendall effect followed by an acid treatment (HF) and an optimized impregnation method. The prepared samples were exhaustively

https://doi.org/10.1021/acs.iecr.3c04045
Ind. Eng. Chem. Res. 2024, 63, 3003−3017

characterized (N_2 physisorption, XRD, SEM, STEM-HAADF, EDX, H_2-TPR, O_2-TPD, XPS, and TPO) and evaluated for total oxidation of DCE at 15,000 h^{-1}. All the modified-oxides exhibited a notable activity, achieving the complete conversion of the pollutant to deep oxidation products at temperatures lower than 330 °C. Ruthenium incorporation enhanced oxygen mobility, both at bulk and surface level, and increased the population of Co^{2+} and O_{ads} species at the surface which upgraded the oxidation activity owing to the large population of available active surface oxygen species. Furthermore, the acid treatment considerably improved the dispersion of the ruthenium by preferentially depositing it on the outermost surface and strengthened the interaction between the noble metal and the cobalt oxide, leading to a remarkable stability (compared with the untreated counterpart) during a relatively prolonged time on stream (120 h) under dry and humid conditions.

■ ASSOCIATED CONTENT

Supporting Information

The Supporting Information is available free of charge at https://pubs.acs.org/doi/10.1021/acs.iecr.3c04045.

N_2 isotherms and pore size distribution of the modified Co_3O_4 catalysts; consecutive light-off runs of the 1Ru/Co_3O_4 catalyst; Raman spectra of the acid-etched and fresh Co_3O_4 catalysts; particle size distribution of the modified Co_3O_4 catalysts; Raman spectra of the modified Co_3O_4 catalysts; and comparison of experimental data and estimated values from conversions of the rate equation at different temperatures (PDF)

■ AUTHOR INFORMATION

Corresponding Author

Rubén López-Fonseca − *Chemical Technologies for Environmental Sustainability Group, Department of Chemical Engineering, Faculty of Science and Technology, University of the Basque Country UPV/EHU, Leioa E-48940 Bizkaia, Spain;* orcid.org/0000-0002-1048-3988; Email: ruben.lopez@ehu.eus

Authors

Amaya Gil-Barbarin − *Chemical Technologies for Environmental Sustainability Group, Department of Chemical Engineering, Faculty of Science and Technology, University of the Basque Country UPV/EHU, Leioa E-48940 Bizkaia, Spain;* orcid.org/0000-0002-1374-8144

José Ignacio Gutiérrez-Ortiz − *Chemical Technologies for Environmental Sustainability Group, Department of Chemical Engineering, Faculty of Science and Technology, University of the Basque Country UPV/EHU, Leioa E-48940 Bizkaia, Spain*

Beatriz de Rivas − *Chemical Technologies for Environmental Sustainability Group, Department of Chemical Engineering, Faculty of Science and Technology, University of the Basque Country UPV/EHU, Leioa E-48940 Bizkaia, Spain*

Complete contact information is available at: https://pubs.acs.org/10.1021/acs.iecr.3c04045

Author Contributions

The manuscript was written through contributions of all authors. All authors have given approval to the final version of the manuscript. All authors contributed equally.

Notes

The authors declare no competing financial interest.

■ ACKNOWLEDGMENTS

This research was funded by the Spanish Ministry of Science and Innovation (PID2022-141583OB-I00 AEI/FEDER, UE and PID2022-141583OB-I00 AEI/FEDER, UE), the Basque Government (IT1509-22), and the University of the Basque Country UPV/EHU (PIF18/185). The authors are grateful for the technical and personal support provided by the SGIker (UPV/EHU). In addition, the authors acknowledge the use of instrumentation as well as the technical advice provided by the National Facility ELECMI ICTS, node "Advanced Microscopy Laboratory" at the University of Zaragoza.

■ ABBREVIATIONS

DCE, 1,2-dichloroethane; DCM, dichloromethane; VC, vinyl chloride; CB, chlorobenzene; DCB, 1,2-dichlorobenzene

■ REFERENCES

(1) Huang, B.; Lei, C.; Wei, C.; Zeng, G. Chlorinated volatile organic compounds (Cl-VOCs) in environment - sources, potential human health impacts, and current remediation technologies. *Environ. Int.* **2014**, *71*, 118−138.

(2) Mu, Y.; Williams, P. T. Recent advances in the abatement of volatile organic compounds (VOCs) and chlorinated-VOCs by non-thermal plasma technology: a review. *Chemosphere* **2022**, *308*, 136481.

(3) Pang, C.; Han, R.; Su, Y.; Zheng, Y.; Peng, M.; Liu, Q. Effect of the acid site in the catalytic degradation of volatile organic compounds: a review. *Chem. Eng. J.* **2023**, *454*, 140125.

(4) Gao, X.; Jiang, X.; Shao, S.; Tu, C.; Pan, J.; Wang, Y.; Zhang, H.; Dai, Q.; Wang, L.; Wang, X. Catalytic oxidation of chlorinated aromatics over Fe-based oxide catalysts modified by Mn. *Chem. Eng. J.* **2022**, *446*, 136771.

(5) Liu, H.; Li, X.; Dai, Q.; Zhao, H.; Chai, G.; Guo, Y.; Guo, Y.; Wang, L.; Zhan, W. Catalytic oxidation of chlorinated volatile organic compounds over Mn-Ti composite oxides catalysts: elucidating the influence of surface acidity. *Appl. Catal., B* **2021**, *282*, 119577.

(6) Xu, S.; Ma, Y. K.; Zhang, K. F.; Jia, A. P.; Chen, J.; Luo, M. F.; Wang, Y.; Lu, J. Q. Catalytic oxidation of dichloromethane over phosphate-modified Co_3O_4: improved performance and control of byproduct selectivity by Co_3O_4 defects and surface acidity. *Appl. Surf. Sci.* **2022**, *606*, 154924.

(7) Chen, X.; Yu, S.; Liu, W.; Zhang, S.; Liu, S.; Feng, Y.; Zhang, X. Recent advance on cobalt-based oxide catalyst for the catalytic removal of volatile organic compounds: a review. *Resour. Chem. Mater.* **2022**, *1* (1), 27−46.

(8) Suo, Y.; Yao, Y.; Zhang, Y.; Xing, S.; Yuan, Z. Y. Recent advances in cobalt-based Fischer−Tropsch synthesis catalysts. *J. Ind. Eng. Chem.* **2022**, *115*, 92−119.

(9) de Rivas, B.; López-Fonseca, R.; Jiménez-González, C.; Gutiérrez-Ortiz, J. I. Highly active behaviour of nanocrystalline Co_3O_4 from oxalate nanorods in the oxidation of chlorinated short chain alkanes. *Chem. Eng. J.* **2012**, *184*, 184−192.

(10) Zhang, W.; Anguita, P.; Díez-Ramírez, J.; Descorme, C.; Valverde, J. L.; Giroir-Fendler, A. Comparison of different metal doping effects on Co_3O_4 catalysts for the total oxidation of toluene and propane. *Catalysts* **2020**, *10*, 865.

(11) Wang, C.; Zhang, C.; Hua, W.; Guo, Y.; Lu, G.; Gil, S.; Giroir-Fendler, A. Low-temperature catalytic oxidation of vinyl chloride over Ru modified Co_3O_4 catalysts. *RSC Adv.* **2016**, *6*, 99577−99585.

(12) Lao, Y.; Zhu, N.; Jiang, X.; Zhao, J.; Dai, Q.; Wang, X. Effect of Ru on the activity of Co_3O_4 catalysts for chlorinated aromatics oxidation. *Catal. Sci. Technol.* **2018**, *8*, 4797−4811.

(13) Hevia, M. A. G.; Amrute, A. P.; Schmidt, T.; Pérez-Ramírez, J. Transient mechanistic study of the gas-phase HCl oxidation to Cl_2 on bulk and supported RuO_2 catalysts. *J. Catal.* **2010**, *276*, 141−151.

(14) Xia, H.; Bai, Y.; Niu, Q.; Chen, B.; Wang, F.; Gao, B.; Liu, L.; Wang, X.; Deng, W.; Dai, Q. Support-dependent activity and thermal stability of Ru-based catalysts for catalytic combustion of light hydrocarbons. *Ind. Eng. Chem. Res.* **2023**, *62*, 1826−1838.
(15) Liu, H.; Yang, J.; Jia, Y.; Wang, Z.; Jiang, M.; Shen, K.; Zhao, H.; Guo, Y.; Guo, Y.; Wang, L.; Dai, S.; Zhan, W. Significant improvement of catalytic performance for chlorinated volatile organic compound oxidation over RuO_x supported on acid-etched Co_3O_4. *Environ. Sci. Technol.* **2021**, *55*, 10734−10743.
(16) Fan, J.; Sun, Y.; Fu, M.; Li, J.; Ye, D. Modulate the metal support interactions to optimize the surface-interface features of Pt/CeO_2 catalysts for enhancing the toluene oxidation. *J. Hazard. Mater.* **2022**, *424*, 127505.
(17) Zhang, C.; Wang, L.; Etim, U. J.; Song, Y.; Gazit, O. M.; Zhong, Z. Oxygen vacancies in Cu/TiO_2 boost strong metal-support interaction and CO_2 hydrogenation to methanol. *J. Catal.* **2022**, *413*, 284−296.
(18) Wan, J.; Chen, W.; Jia, C.; Zheng, L.; Dong, J.; Zheng, X.; Wang, Y.; Yan, W.; Chen, C.; Peng, Q.; Wang, D.; Li, Y. Defect effects on TiO_2 nanosheets: stabilizing single atomic site Au and promoting catalytic properties. *Adv. Mater.* **2018**, *30*, 1705369.
(19) Gong, X. Q.; Selloni, A.; Dulub, O.; Jacobson, P.; Diebold, U. Small Au and Pt clusters at the anatase TiO_2(101) surface: behavior at terraces, steps and surface oxygen vacancies. *J. Am. Chem. Soc.* **2008**, *130* (1), 370−381.
(20) Dai, W.; Li, C.; Wang, F.; Zhang, C.; Liu, P.; Qiao, H.; Li, Z. Engineering surface Mn-enricher species and regulating active oxygen species over $LaMnO_3$ catalysts by synergistic modification of acid etching and potassium support for soot removal. *New J. Chem.* **2022**, *46*, 22283−22293.
(21) Dai, L.; Lu, X. B.; Chu, G. H.; He, C. H.; Zhan, W. C.; Zhou, G. J. Surface tuning of $LaCoO_3$ perovskite by acid etching to enhance its catalytic performance. *Rare Met.* **2021**, *40* (3), 555−562.
(22) Gil-Barbarin, A.; Gutiérrez-Ortiz, J. I.; López-Fonseca, R.; de Rivas, B. Co_3O_4 hollow nanotubes for the catalytic oxidation of C_2-chlorinated VOCs. *J. Environ. Chem. Eng.* **2023**, *11*, 109841.
(23) Zheng, C.; Li, H.; Yang, Y.; Zhang, S.; Yu, X.; Xin, Q.; Liu, S.; Gao, X. Promotional effects of ruthenium oxide on catalytic oxidation of dichloromethane over the tungsten-titanium binary oxides catalyst. *Proc. Combust. Inst.* **2021**, *38*, 6461−6471.
(24) Wang, G.; Liu, H.; Horvat, J.; Wang, B.; Qiao, S.; Park, J.; Ahn, H. Highly ordered mesoporous cobalt oxide nanostructures: synthesis, characterisation, magnetic properties and applications for electrochemical energy devices. *Chem.—Eur. J.* **2010**, *16*, 11020−11027.
(25) Pudukudy, M.; Yaakob, Z.; Narayanan, B.; Gopalakrishnan, A.; Tasirin, S. M. Facile synthesis of bimodal mesoporous spinel Co_3O_4 nanomaterials and their structural properties. *Superlattices Microstruct.* **2013**, *64*, 15−26.
(26) Yoo, S.; Lee, E. W.; Kim, D. H. Methane combustion over mesoporous cobalt oxide catalysts: effects of acid treatment. *Mol. Catal.* **2021**, *511*, 111728.
(27) Stuchinskaya, T. L.; Musawir, M.; Kozhevnikova, E. F.; Kozhevnikov, I. V. Liquid-phase oxidation of alcohols by oxygen and nitrous oxide catalysed by Ru-Co oxide. *J. Catal.* **2005**, *231*, 41−47.
(28) Song, W.; Poyraz, A. S.; Meng, Y.; Ren, Z.; Chen, S. Y.; Suib, S. L. Mesoporous Co_3O_4 with controlled porosity: inverse micelle synthesis and high-performance catalytic CO oxidation at - 60 °C. *Chem. Mater.* **2014**, *26*, 4629−4639.
(29) Tian, M.; Jiang, Z.; Chen, C.; Kosari, M.; Li, X.; Jian, Y.; Huang, Y.; Zhang, J.; Li, L.; Shi, J. W.; Zhao, Y.; He, C. Engineering Ru/$MnCo_3O_x$ for 1,2-dichloroethane benign destruction by strengthening C-Cl cleavage and chlorine desorption: decisive role of H_2O and reaction mechanism. *ACS Catal.* **2022**, *12*, 8776−8792.
(30) Zhu, W.; Chen, X.; Jin, J.; Di, X.; Liang, C.; Liu, Z. Insight into catalytic properties of Co_3O_4-CeO_2 binary oxides for propane total oxidation. *Chin. J. Catal.* **2020**, *41*, 679−690.
(31) Zhang, W.; Li, M.; Wang, X.; Zhang, X.; Niu, X.; Zhu, Y. Boosting catalytic toluene combustion over Mn doped Co_3O_4 spinel catalysts: Improved mobility of surface oxygen due to formation of Mn-O-Co bonds. *Appl. Surf. Sci.* **2022**, *590*, 153140.
(32) Choya, A.; Gudyka, S.; de Rivas, B.; Gutiérrez-Ortiz, J. I.; Kotarba, A.; López-Fonseca, R. Design, characterization and evaluation of Ce-modified cobalt catalysts supported on alpha alumina in the abatement of methane emissions from natural gas engines. *Appl. Catal., A* **2021**, *617*, 118105.
(33) Zeng, K.; Li, X.; Wang, C.; Wang, Z.; Guo, P.; Yu, J.; Zhang, C.; Zhao, X. S. Three-dimensionally microporous $MnZrO_x$ catalysts for propane combustion: synergistic structure and doping effects on physicochemical and catalytic properties. *J. Colloid Interface Sci.* **2020**, *572*, 281−296.
(34) Sui, C.; Zhang, T.; Dong, Y.; Yuan, F.; Niu, X.; Zhu, Y. Interaction between Ru and Co_3O_4 for promoted catalytic decomposition of N_2O over the Ru_x-Co_3O_4 catalysts. *Mol. Catal.* **2017**, *435*, 174−181.
(35) Wang, Y.; Du, Y.; Fu, Z.; Wang, M.; Fu, Y.; Li, B.; Wang, L. External and internal dual-controls: Tunable cavity and Ru-O-Co bond bridge synergistically accelerate the RuCoCu-MOF/CF nanorods for urea-assisted energy-saving hydrogen production. *Int. J. Hydrogen Energy* **2023**, *48*, 23412−23424.
(36) Sun, W.; Gong, B.; Pan, J.; Wang, Y.; Xia, H.; Zhang, H.; Dai, Q.; Wang, L.; Wang, X. Catalytic combustion of CVOCs over Cr_xTi_{1-x} oxide catalysts. *J. Catal.* **2020**, *391*, 132−144.
(37) López-Fonseca, R.; Gutiérrez-Ortiz, J.; Gutiérrez-Ortiz, M.; González-Velasco, J. Catalytic combustion of chlorinated ethylenes over H-zeolites. *J. Chem. Technol. Biotechnol.* **2003**, *78*, 15−22.
(38) Li, Y.; Hu, F. P.; Wang, X.; Shen, P. K. Anchoring metal nanoparticles on hydrofluoric acid treated multiwalled carbon nanotubes as stable electrocatalysts. *Electrochem. Commun.* **2008**, *10*, 1101−1104.
(39) Li, J.; Zhang, R.; Liu, Y.; Sun, T.; Jia, J.; Guo, M. Enhanced catalytic activity of toluene oxidation over in-situ prepared Mn_3O_4-Fe_2O_3 with acid-etching treatment. *Catal. Commun.* **2023**, *174*, 106581.
(40) Liu, Q.; Wang, L. C.; Chen, M.; Cao, Y.; He, H. Y.; Fan, K. N. Dry citrate-precursor synthesized nanocrystalline cobalt oxide as highly active catalyst for total oxidation of propane. *J. Catal.* **2009**, *263*, 104−113.
(41) Park, J. Y.; Lee, Y. J.; Karandikar, P. R.; Jun, K. W.; Bae, J. W.; Ha, K. S. Ru promoted cobalt catalyst on γ-Al_2O_3 support: Influence of pre-synthesized nanoparticles on Fischer−Tropsch reaction. *J. Mol. Catal. A: Chem.* **2011**, *344*, 153−160.
(42) Lu, Q.; Guo, Y.; Mao, P.; Liao, K.; Zou, X.; Dai, J.; Tan, P.; Ran, R.; Zhou, W.; Ni, M.; Shao, Z. Rich atomic interfaces between sub-1 nm RuO_x clusters and porous Co_3O_4 nanosheets boost oxygen electrocatalysis bifunctionality for advanced Zn-air batteries. *Energy Storage Mater.* **2020**, *32*, 20−29.
(43) Miranda, B.; Díaz, E.; Ordóñez, S.; Vega, A.; Díez, F. V. Oxidation of trichloroethene over metal oxide catalysts: Kinetic studies and correlation with adsorption properties. *Chemosphere* **2007**, *66*, 1706−1715.
(44) Zhang, H.; Wang, S.; Wang, M.; Li, G.; Yu, L.; Liu, X.; Wang, Z.; Zhang, C. Catalytic oxidation of vinyl chloride over Co-Ce composite oxides derived from ZIF-67 template: Effect of cerium incorporation. *J. Rare Earths* **2023**, *41* (6), 870−880.
(45) Hu, Z.; Chen, J.; Yan, D.; Li, Y.; Jia, H.; Lu, C. Z. Enhanced catalytic activities of MnO_x/Co_3O_4 nanocomposites prepared via MOFs-templated approach for chlorobenzene oxidation. *Appl. Surf. Sci.* **2021**, *551*, 149453.
(46) Hua, W. C.; Li, M. Q.; Guo, Y. L.; Chai, G. T.; Liu, H.; Guo, Y.; Wang, L.; Zhan, W. C. Catalytic combustion of vinyl chloride emissions over Co_3O_4 catalysts with different crystallite sizes. *Rare Met.* **2021**, *40*, 817−827.
(47) Deng, W.; Jia, Z.; Gao, B.; Zhu, S.; Liu, D.; Guo, L. Effect of preparation method on the performance of porous RuO_x/Co_3O_4 catalysts for 1,2-dichloroethane oxidation. *Appl. Catal., A* **2021**, *624*, 118300.

https://doi.org/10.1021/acs.iecr.3c04045
Ind. Eng. Chem. Res. 2024, 63, 3003−3017

(48) Liu, X.; Zeng, J.; Shi, W.; Wang, J.; Zhu, T.; Chen, Y. Catalytic oxidation of benzene over ruthenium-cobalt bimetallic catalysts and study of its mechanism. *Catal. Sci. Technol.* **2017**, *7*, 213−221.
(49) Liu, X.; Wang, J.; Zeng, J.; Wang, X.; Zhu, T. Catalytic oxidation of toluene over a porous Co_3O_4-supported ruthenium catalyst. *RSC Adv.* **2015**, *5*, 52066−52071.
(50) Yan, J.; Wang, L.; Guo, Y.; Guo, Y.; Dai, Q.; Zhan, W. Comparisons on thermal and water-resistance of Ru and Pd supported on cobalt-doped alumina nanosheets for catalytic combustion of propane. *Appl. Catal., A* **2021**, *628*, 118398.
(51) Yang, P.; Zuo, S.; Zhou, R. Synergistic catalytic effect of $(Ce,Cr)_xO_2$ and HZSM-5 for elimination of chlorinated organic pollutants. *Chem. Eng. J.* **2017**, *323*, 160−170.
(52) Shi, Y.; Guo, X.; Shi, Z.; Zhou, R. Transition metal doping effect and high catalytic activity of CeO_2-TiO_2 for chlorinated VOCs degradation. *J. Rare Earths* **2022**, *40*, 745−752.
(53) Huang, Y.; Fang, S.; Tian, M.; Jiang, Z.; Wu, Y.; He, C. Chlorine-resistant hollow nanosphere-like VO_x/CeO_2 catalysts for highly selective and stable destruction of 1,2-dichloroethane: byproduct inhibition and reaction mechanism. *Processes* **2021**, *9* (1), 119.

https://doi.org/10.1021/acs.iecr.3c04045
Ind. Eng. Chem. Res. 2024, 63, 3003−3017